Thermo-Hydraulic-Mechanical Modelling of the Full-Scale Emplacement (FE) Experiment at the Mont Terri Rock Laboratory – 16490

Kate Thatcher*, Alex Bond*, Benoit Garitte**, Tobias Vogt** and Herwig R. Müller**

* Quintessa Ltd, UK

** Nagra, Switzerland

ABSTRACT

The Full-Scale Emplacement Experiment at the Mont Terri underground research laboratory is a heater test carried out in a gallery constructed in Opalinus Clay. The aim of the experiment is both to develop emplacement procedures for radioactive waste canisters and their surrounding backfill as well as understanding the thermo-hydro-mechanical effects of disposing of radioactive waste on the engineering materials and the host rock.

Coupled thermo-hydro-mechanical models have been used to aid planning of the locations of sensors, to inform decisions on the schedule for turning on the heaters as well as to make predictions of the temperatures and water pressures in the bentonite and the Opalinus Clay. The FE Experiment was preceded by a number of other experiments at the Mont Terri laboratory at smaller scales, but with similar materials, which provided crucial input to the models and gave confidence in the general process understanding.

Blind predictions were made prior to turning on the heaters, of the temperature and relative humidity in the bentonite surrounding the heaters. The comparison between the blind predictions and early data from the experiment show that knowledge gained from smaller scale experiments on similar materials has enabled good blind predictions to be made and gives confidence that temperature in the experiment is unlikely to rise to a level that could damage the sensors. It also demonstrates that the thermal properties of the disposal system are understood well enough to produce reliable estimates of temperature in the backfill.

INTRODUCTION - THE FE EXPERIMENT

The design of the Full-Scale Emplacement (FE) Experiment at the Mont Terri underground research laboratory (URL) is is based on the Swiss disposal concept for spent fuel (SF) and vitrified high-level waste (HLW) [1]. The FE experiment consists of three heaters, with dimensions similar to those of waste canisters, emplaced in a shotcrete-lined tunnel onto pedestals made from bentonite blocks. The remaining space within the tunnel was backfilled with granulated bentonite mixture (GBM) and the tunnel was then sealed with a concrete plug. The 4.6m long heaters were turned on over a period of 3 months starting in December 2014 and are currently running at 1350 Watt each (Fig. 1, 2). Alongside testing the

(horizontal) canister and GBM emplacement procedures at underground conditions, a key aim of the experiment is to investigate SF / HLW repository-induced thermo-hydraulic-mechanical (THM) effects on the bentonite and the host rock. To enable this investigation, several hundred sensors have been installed within the tunnel and host rock to measure the THM response of the system. The experiment is expected to run for at least 10 to 15 years.

This paper presents a brief overview of the THM analysis that was performed in preparation for the FE design and construction. These models were then used to provide a full blind prediction of the THM behaviour of the experiment; the blind comparison of the models and early data from the FE are also discussed.

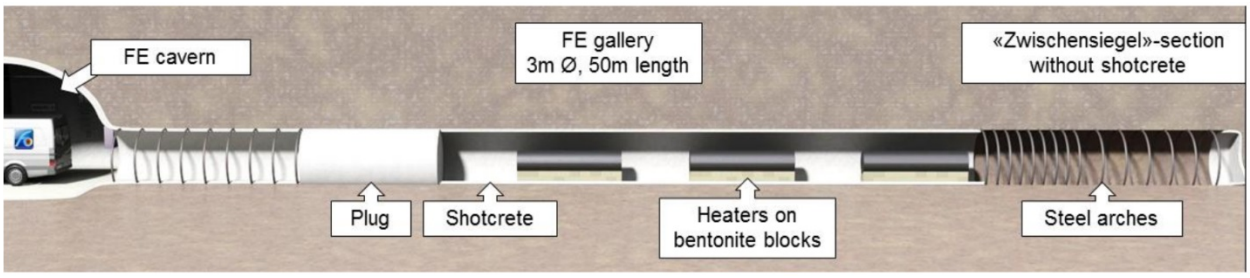

Fig. 1. FE Experiment Geometry (section view). Sensors and backfill are not shown.

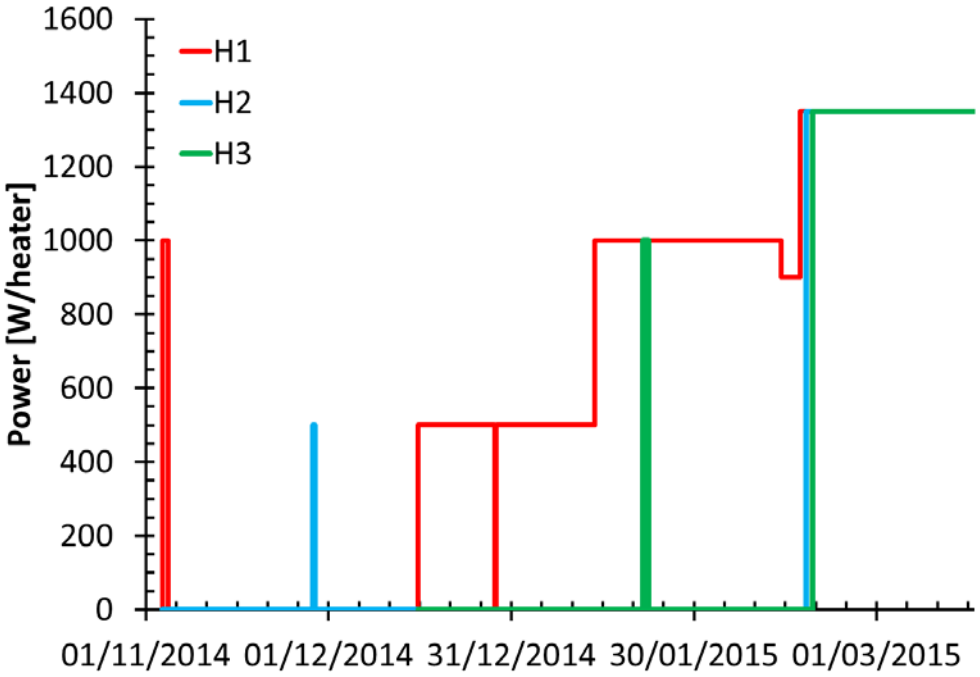

Fig. 2. Planned heating schedule for the first five months, following the preparatory modelling.

THM PREPARATORY MODELLING

Modelling Objectives and Approach

The primary purpose of the modelling was to aid in the experimental design, particularly the power loading applied to the heaters. Ensuring that the temperatures were not too high was important because a number of the sensors are particularly temperature sensitive, and excessive temperatures could result in their premature failure. Such work necessarily involves blind prediction of the THM system response, hence building up confidence in the constitutive models and the modelled implementation was of prime importance.

The modelling approach took the following steps:

1. Compilation of work conducted on the preceding HE-E and HE-D experiments, with particular focus on derived thermal properties with water saturation [2],[3].
2. Demonstration that the implementation of the constitutive models in QPAC gave equivalent results to previous models.
3. Successful participation in 1D axi-symmetric code benchmarking with other modelling participants in the FE project.
4. Use of heater 'calorimeter' tests and an in-situ 24 hour heater test to: further constrain the model parameterisation; define the experimental power protocol, and; make final 3D predictions of THM behaviour.

This paper covers the results of point 4 in the process.

Constitutive Relationships and Numerical Formulation

The thermal and hydraulic process conceptual model for the system is shown in Fig. 3.

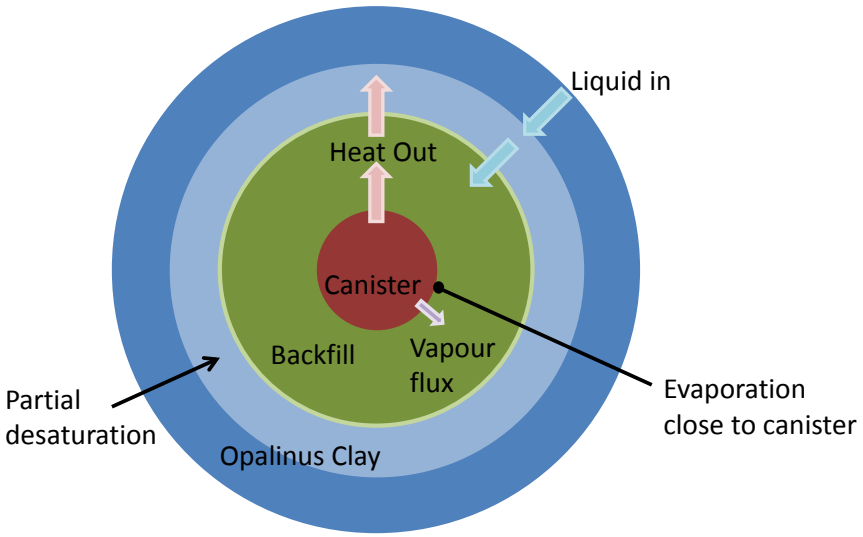

Fig. 3. Conceptual model for the thermal and hydraulic evolution of the FE experiment

A conventional finite volume (or control volume) approximation was adopted [4]. In the finite volume method, volume integrals in a partial differential equation that contain a divergence term can be converted to surface integrals, using the divergence theorem, enabling the original partial differential equation to be replaced by ordinary differential equations for the volume-averaged variables. The Darcy multi-phase flow, vapour transport, thermal conduction and continuum mechanics equations can be readily transferred into the control volume framework and a brief summary of the relevant relationships is provided below.

For the fluid transfers, we specify that the fluids occupy the total available pore space such that the fractional volume occupancy of each phase (saturation – *S*) sums to unity, i.e.

$$S_w + \sum_{nw} S_{nw} = 1 \qquad (1)$$

where the subscript *w* denotes the wetting phase (water) and *nw* is a non-wetting phase. For this analysis we assume there is one wetting phase (water) and one non-wetting phase (air). The difference in pressure (*p* – MPa) between the wetting and non-wetting phase is normally termed the capillary pressure or suction (p_c) and for a two-phase system is defined as a function of the saturation of the wetting phase:

$$p_w = p_{nw} - p_c(S_w) \qquad (2)$$

If we denote the fluid accessible porosity of the porous medium by θ (-) and the density of phase *k* by ρ_k (kg m^{-3}), then $\theta\rho_k S_k$ (kg m^{-3}) is a conserved quantity in any representative volume of porous media, which inversely relates changes in density to changes in porosity or saturation. If the Darcy velocity of fluid *k* is denoted $\mathbf{u}_k$ (m s^{-1}), the vapour flux or dissolved gas flux is denoted by $\mathbf{v}_k$ (kg m^{-2} s^{-1}) then we can write the equation for the conserved quantity as

$$\frac{\partial}{\partial t}(\theta\rho_k S_k) = -\nabla \cdot (\rho_k \mathbf{u}_k + \mathbf{v}_k) + q_k \qquad (3)$$

where q_k (kg m^{-3} s^{-1}) is a source or sink rate of fluid per unit volume. This basic conservation equation can be directly related to equation (1).

The Darcy velocity of a specific fluid in a multiphase flow setting is given by a simple extension of Darcy's law for single phase flow [5].

$$\mathbf{u}_k = -\frac{\mathbf{k}_k(S_k)}{\mu_k}\nabla(p_k + \rho_k g z) \qquad (4)$$

Here, g (m s^{-2}) is the acceleration due to gravity, z (m) is the vertical coordinate and μ_k (Pa s) is the viscosity of fluid *k*. $\mathbf{k}_k$ (m^2) is the effective permeability tensor of the porous medium for fluid *k* which is a function of fluid saturation. The vapour flux $\mathbf{v}_w$ and dissolved gas flux $\mathbf{v}_{nw}$ are defined as follows

$$\mathbf{v}_w = -D_v(S_w)\nabla\rho_v \qquad (5)$$

$$\mathbf{v}_{nw} = -D_{nw}(S_w)\nabla c_{nw} + \mathbf{u}_w c_{nw} \qquad (6)$$

where D_v is the net vapour diffusivity ($m^2\ s^{-1}$), ρ_v is the vapour density (directly related to the capillary pressure; [6]), D_{nw} is the net diffusivity of the non-wetting phase (air) in water ($m^2\ s^{-1}$) and c_{nw} is the concentration of the non-wetting phase in water ($kg\ m^{-3}$).

Thermal heat transfer was modelled as a conductive process:

$$\frac{\partial \rho c T}{\partial t} = \nabla \cdot (\lambda \nabla T) + H \quad (7)$$

where T (K) is the temperature, H (W/m^3) is an external heat source, and ρ ($kg\ m^{-3}$), c ($J\ kg^{-1}\ K^{-1}$) and λ ($W\ m^{-1}\ K^{-1}$) are the density, specific heat capacity and thermal conductivity of the medium respectively. Advective, radiative and latent heat transfers were eliminated as not being significant for this particular case in early prototyping work.

Solid poro-mechanical representations were also investigated for this work using classical effective stress coupling [7], however early work in comparing modelling approaches with work for the HE-E and HE-D showed that a much simpler approach was viable. This alternative approach modifies the effective porosity in equation (3) to account for both poro-elasticity and thermal effects – essentially an extension of the classical approach to storativity in poro-elastic materials (e.g. [8]). The approach assumes that thermal strains in the rock skeleton can be accommodated elsewhere, distant from the heat source.

$$\theta = \theta_0(1 + \Delta T\, \chi) e^{(\nu(P - P_0))/(\theta_0(1 + \Delta T\, \chi))} \quad (8)$$

where θ_0 is the reference porosity, χ is the volumetric thermal expansion coefficient of the rock skeleton and rock grains (K^{-1}), P is the effective fluid pressure (MPa), P_0 is the reference effective fluid pressure (MPa) and ν is the rock bulk compressibility (MPa^{-1}). Water density changes are handled directly via the saturation constraint equation (eqn 1-3). In this instance the Rowe-Chou equation of state for water was used [9]

For this study, a formulation of the above relationships that has been successfully used in a range of other applications was adopted [10],[11],[12],[13],[14]. In this formulation the primary conserved variables are the masses of fluid and heat in each control volume, while the fluid pressures, capillary pressure and temperature are calculated as algebraic variables through the fluid compressibility and rock matrix elasticity terms while satisfying the saturation constraint equation (equation 1), giving rise to six unknowns per control volume.

The equations are solved using a monolithic, fully implicit technique, implemented in 'QPAC', a proprietary multi-physics code developed by Quintessa Ltd [15]; www.quintessa.org/qpac). Non-linear iterations for each time step are solved using a Newton-Raphson scheme while the linearised equations are solved using a GMRES iterative solver. Time-stepping is managed using a polynomial history-derived predictor-corrector method based on the work of [16].

Parameterisation

The hydraulic properties used for the porous media are given in Table I.

The relationship between permeability and water saturation for Opalinus Clay and shotcrete is given by:

$$k_r = S_e^{1/2}\left[1-\left(1-S_e^{1/0.52}\right)^{0.52}\right]^2 \qquad (9)$$

where S_e is the effective saturation given by

$$S_e = \frac{S_w - S_{ir}}{1 - S_{ir}} \qquad (10)$$

where S_w is the water saturation and S_{ir} is the irreducible saturation of water.

The relative permeability of the GBM and bentonite blocks is given by $k_r = S_e^5$.

The relationship between suction (p_c) and water saturation (S_w) for the GBM, bentonite blocks, Opalinus Clay and the shotcrete is given by a van Genuchten equation with parameters as shown in Table I:

$$S_w = \left(\left(1+\left({}^{p_c}/_{p_0}\right)^{\left({}^{1}/_{1-\lambda_0}\right)}\right)^{-\lambda_0}\right) \qquad (11)$$

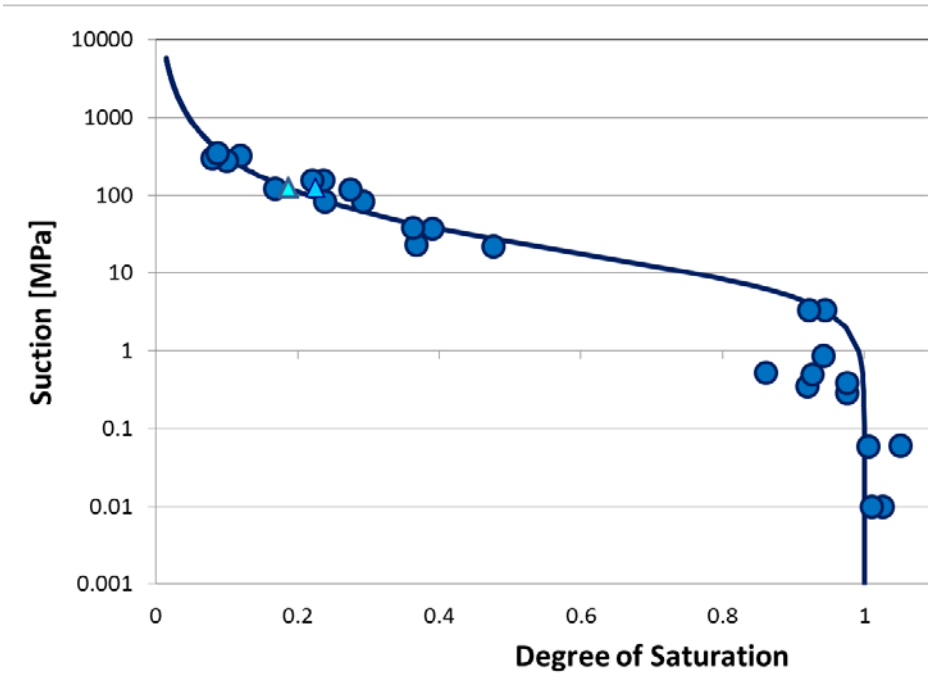

Fig. 4. Water retention curve for bentonite GBM.

The thermal properties used for the porous media are given in Table II.

The bulk density of the material in a given compartment with volume $CompVol$ is calculated by:

$$\rho_{bulk} = \left(M_{grains} + M_{LiquidWat} + M_{WatVap} + M_{Air}\right)/CompVol \qquad (12)$$

where M_i is the mass of material i in the compartment.

The bulk specific heat capacity in a compartment is calculated by a simple mass average:

$$c = \left(c_{grains}M_{grains} + c_{LiquidWat}M_{LiquidWat} + c_{WatVap}M_{WatVap} + c_{Air}M_{Air}\right)/M_{Total}. \qquad (13)$$

The bulk thermal conductivity in the Opalinus Clay, shotcrete and bentonite blocks is calculated as a function of saturation (S_w):

$$\lambda = \lambda_{sat}\sqrt{S_w} + \lambda_{dry}(1 - \sqrt{S_w}) \qquad (14)$$

where λ_{sat} is the saturated thermal conductivity and λ_{dry} is the dry thermal conductivity. The thermal conductivity for the GBM was calculated using the following relationship based on the underpinning data and model calibration:

$$\lambda = \lambda_{sat}^{S_w} + \lambda_{dry}^{(1-S_w)} \qquad (15)$$

TABLE I. Hydraulic Properties for the reference FE model

Parameter	**Value**
Porosity	**-**
Opalinus Clay	0.162
Shotcrete	0.162
GBM	0.475
Bentonite Blocks	0.331
Compressibility	***Pa^{-1}***
Opalinus Clay	1.67E-10
Shotcrete	1.67E-10
GBM	3.33E-9
Bentonite Blocks	1.33E-9
Permeability	***m^2***
Opalinus Clay bedding parallel Opalinus Clay bedding perp	7.54x10^{-20} 7.54x10^{-21}
Shotcrete	3.5E-20
GBM	3.5E-21
Bentonite Blocks	3.5E-21
Capillary Curve	
p_0 Opalinus clay and	11 MPa

shotcrete	
p_0 GMB and bentonite blocks	10 MPa
λ_0 Opalinus clay and shotcrete	0.29
λ_0 GMB and bentonite blocks	0.4
Reference Vapour Diffusivity	***m^2 s^{-1}***
All media	2.68E-5

TABLE II. Thermal Properties for the reference FE model

Parameter	**Value**
Reference Grain Density	***kg m^{-3}***
Opalinus Clay	2700
Shotcrete	2700
GBM	2700
Bentonite Blocks	2700
Specific heat capacity solid grain	***J kg^{-1} K^{-1}***
Opalinus Clay	800
Shotcrete	800
GBM	950
Bentonite Blocks	950
Saturated Thermal conductivity	***W m^{-1} K^{-1}***
Opalinus Clay bedding parallel Opalinus Clay bedding perp	2.15 1.2
Shotcrete	1.70
GBM	1
Bentonite Blocks	1.2
Dry Thermal conductivity	***W m^{-1} K^{-1}***
Opalinus Clay	1.06
Shotcrete	1.06
GBM	0.3
Bentonite Blocks	0.3
Volumetric thermal expansion coefficient (rock skeleton and rock grain)	*K^{-1}*

Model Geometries

Two model variants were considered. The first was a 3D representation of the full FE experiment, including explicit consideration of the desaturation occurring during construction through forced air ventilation (Fig. 5). The second was a more detailed modelling of heater 1 (the furthest from the access drift), when the buffer was partially installed, for the 24 hour heater test (Fig. 6). The models were developed in parallel and the results of the 24 hour heater test calibration used to inform the full FE model. In all cases, outer boundaries were specified pressure (hydrostatic) and background temperature at 45 m from the centre of the gallery.

A key uncertainty was the treatment of the heater in the model. The reference assumption was that a solid cylinder, with an adjusted density to give the correct mass, would be appropriate as the thermal conductivity of the steel shell of the heat was sufficiently high the heat source within the canister would be homogenised. However, work on the 24 hour heater test showed that treating the heater as constructed, with a thin steel shell, gave significantly different results below the heater, depending on the assumptions of regarding the thermal parameterisation of the compacted bentonite blocks. This difference in heater representation was expected to become less significant over longer timescales given the reference thermal parameterisation, so the full model used the solid cylinder model. Ongoing work will investigate the sensitivity of the alternative heater representation.

The underpinning thermal conductivity data showed considerable uncertainty in the ‘dry’ thermal conductivity of the GBM. This uncertainty was reflected in the model runs by running two variants; ‘lowTC’ – dry thermal conductivity of 0.2 W/m/K; and ‘highTC’ – dry thermal conductivity of 0.4 W/m/K.

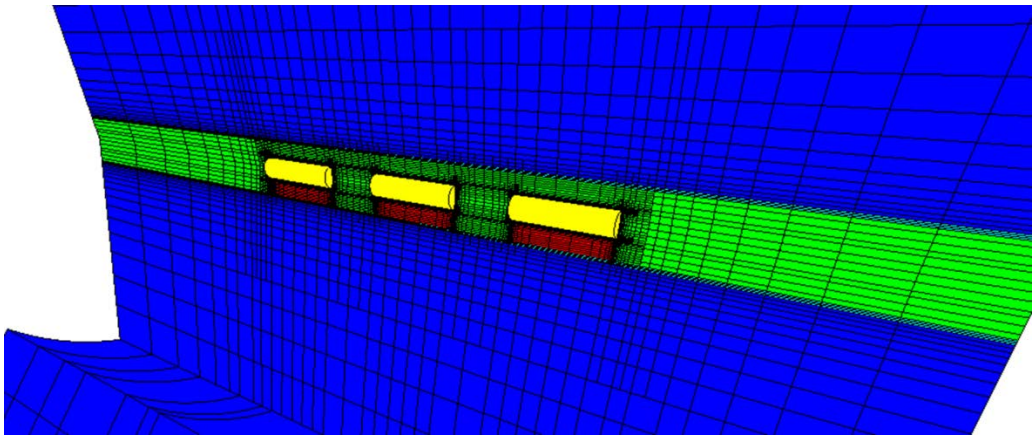

Fig 6. Model grid showing 3 heaters resting on the pedestals for the complete FE experiment. Green is the GBM, yellow the heaters, red the compacted bentonite blocks, pale blue the shotcrete liner and dark blue the Opalinus clay.

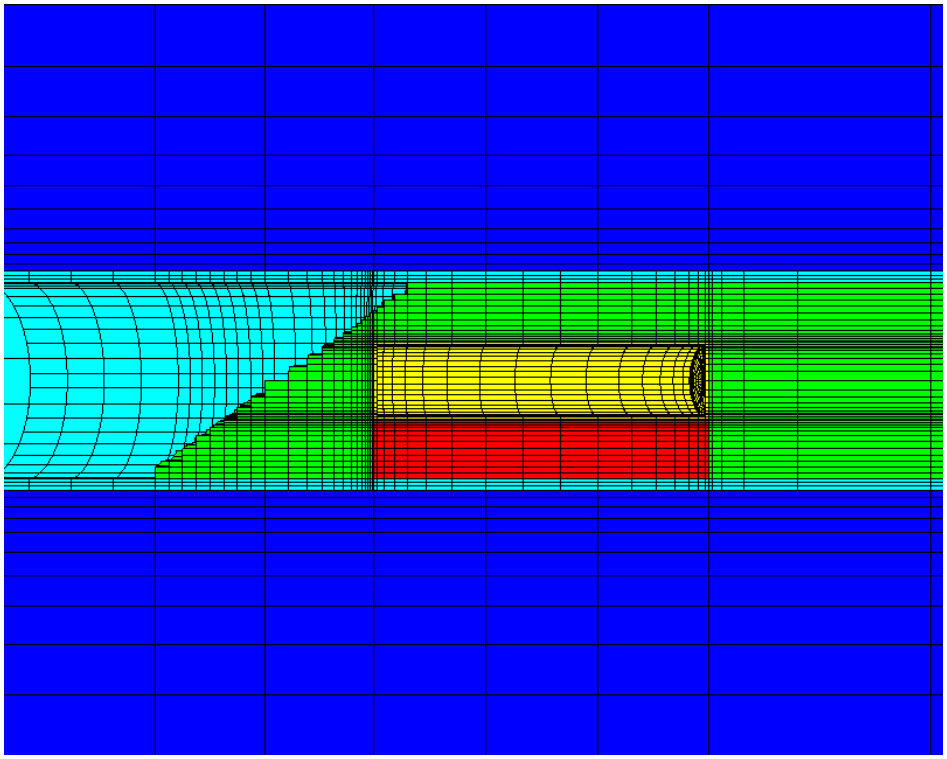

Fig 7. Grid around the heater when using the hollow shell heater model for the 24 hour heater test. Green is the GBM, yellow the heaters, red the compacted bentonite blocks, pale blue the shotcrete liner and dark blue the Opalinus clay.

COMPARISON OF BLIND PREDICTIONS AGAINST EARLY FE DATA

In general, the temperatures observed in the experiment fall within or close to the boundaries of the temperatures predicted by the modelling, with temperatures at the sides and above the heater lying very close to the base case model prediction (Fig. 7 and Fig. 8).

Fig. 9 shows that the model predicted the peak temperature on the surface of heater 1 (H1) accurately over the first few months of the experiment. There were fewer data available for H2 and H3 as they were switched on at a later date than H1. However, the model predictions for H1 are consistent with the data collected thus far for H2 and H3

The model results show the same temperature at the heater surface in all four angular directions for all three heaters. The data from the experiment show consistently lower temperatures in the vertically downwards direction and slightly higher temperatures in the vertically upwards direction as compared to the horizontal directions.

Temperatures 10 cm outside the heater within the GBM at the sides of the heater fall within the range of the model predictions, as seen in Fig. 8. However, the model does not predict the temperature in the bentonite blocks beneath the heater and in the GBM above the heater as well as it does on the surface of the heater - the temperature is slightly lower than the model predicts. Some of this error is thought to occur due to the thermal parameters used for the bentonite blocks. Work is ongoing to resolve these inconsistencies.

Fig. 10 shows that the measured values for relative humidity in the GBM are similar to the modelled results given by QPAC. However, the model over-predicts the relative humidity in the bentonite blocks. This is thought to be due to an inconsistency in the actual bentonite blocks as installed and the planned material, particularly with respect to the final water content and retention curves. An improved characterisation of the blocks in the model relative to the experiment is a key priority for ongoing work.

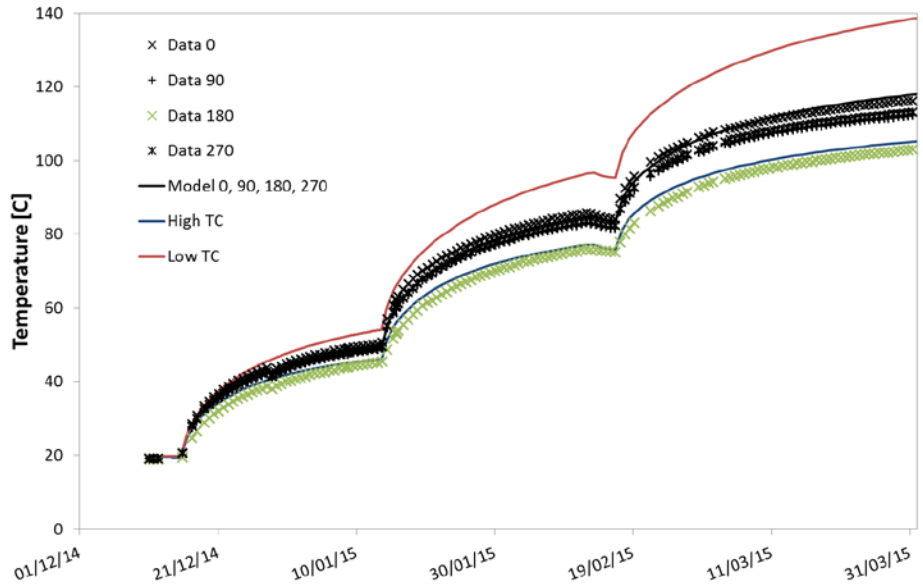

Fig 8. Temperature data (symbols) and model predictions (lines) for the surface of heater 1.

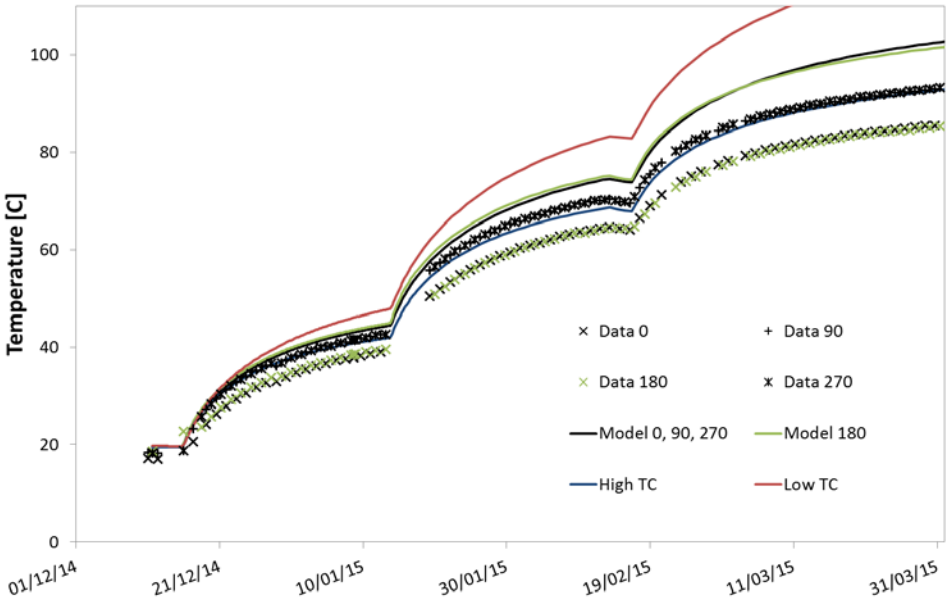

Fig 9. Temperature data (symbols) and model predictions (lines) 10 cm from the surface of heater 1.

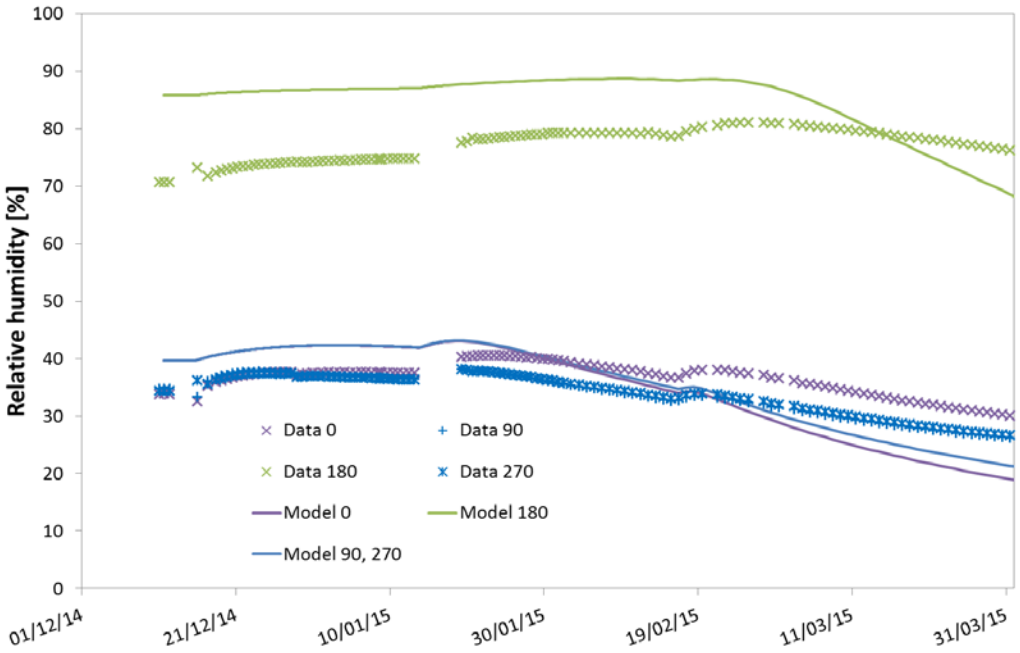

Fig 10: Relative humidity data (symbols) and model predictions (lines) for 10 cm away from the surface of heater 1.

CONCLUSIONS

A series of models and experiments underpinning the FE experiment have enabled good blind predictions temperature around the installed heaters to be made, despite considerable uncertainties in the coupled thermal-hydraulic parametrisation of the GBM and the bentonite blocks.

Work on the 24 hour heater test showed that temperatures close to the heater can be improved by representing the heater as a hollow shell rather than a solid volume. The 24 hour heater test also revealed that some calibration of the thermal properties of the bentonite blocks and GBM would improve the fit between the model and the data. Further work is therefore planned to improve the thermal predictions close to the heater by using the 24 hour heater test (which has much shorter run times) to further improve the parameterisation of the bentonite thermal properties. In particular, it is considered useful to do some inverse modelling to determine the relationship between the thermal conductivity of the bentonite blocks and the GBM to improve the distribution of heat around the canister.

There is a general need to improve the representation of the bentonite blocks, as there is evidence that the initial thermal and hydraulic parameterisation is inconsistent with the ‘as-built’ condition of the FE experiment. Along the with the heater representation this is a priority for future modelling work.

The work here has focussed on temperature close to the heater, but further consideration will be made of temperatures further from the heater both within the

tunnel and in the Opalinus Clay as the thermal pulse develops and the hydraulic influence of the heat sources are felt.

REFERENCES

1. Müller, H.R., Garitte, B., Köhler, S., Vogt, T., Sakaki, T., Weber, H. and Vietor, T. (2015). LUCOEX – Final report of WP2. Deliverable D2.6
2. Garitte, B., Gens, A., Vaunat, J., & Armand, G. (2012): Thermal conductivity of argillaceous rocks: Determination methodology using in-situ heating tests. Rock Mech Rock Eng, DOI 10.1007/s00603-012-0335-x
3. Gaus, I., Garitte, B., Senger, R., Gens, A., Vasconcelos, R., Garcia-Sineriz, J.-L., Trick, T., Wieczorek, K., Czaikowski, O., Schuster, K., Mayor, J.C., Velasco, M., Kuhlmann, U. and Villar, M.V. (2014). The HE-E Experiment: Lay-out, Interpretation and THM Modelling. Nagra Report NAB 14-53.
4. Versteeg H and Malalasekra W (2007). An Introduction to Computational Fluid Dynamics: The Finite Volume Method (2nd Edition). Pearson Education Limited
5. Chen Z, Huan G and Ma Y (2006). Computational Methods for Multiphase Flows in Porous Media. SIAM, Society for Industrial and Applied Mathematics, Philadelphia. http://dx.doi.org/10.1137/1.9780898718942
6. Engel J, Schanz T and Lauer C (2003). State Parameters for Unsaturated Soils, Basic Empirical Concepts. Proc. Int. Conf. From Experimental Evidence towards Numerical Modeling of Unsaturated Soils, Weimar, Germany, 2003 (ed. T. Schanz), Berlin: Springer, Vol. 2, pp. 125-138.
7. Bishop AW. (1959) The principle of effective stress. Tecnisk Ukeblad;106(39):859–63.
8. Fetter CW (1994). Applied Hydrogeology 3rd Edition, Prentice-Hall. ISBN 0-02-336490-4.
9. Rowe A and Chou J (1970). Pressure-Volume-Temperature Relation of Aqueous NaCl Solutions. J. Chem. Eng. Data, 15: 61-66.
10. Benbow SJ, Rivett MO, Chittenden N, Herbert AW, Watson S, Williams SJ and Norris S (2014). Potential migration of buoyant LNAPL from Intermediate Level Waste (ILW) emplaced in a geological disposal facility (GDF) for UK radioactive waste. J. Contam. Hydrol., 167 (2014), 1-22 http://dx.doi.org/10.1016/j.jconhyd.2014.07.011
11. Bond AE, Metcalfe R, Maul PR, Suckling P, Thatcher KE, Walke R, Smith K, Rasse D, Steven M and D Jones (2013a). Systems analysis of field and laboratory experiments considering impacts of CO2 leakage in terrestrial systems. Energy Procedia 37 (2013) 3394-3402. http://dx.doi.org/10.1016/j.egypro.2013.06.228
12. Bond A, Millard A, Nakama S, Zhang C, Garitte B. (2013b) Approaches for representing hydromechanical coupling between large engineered voids and argillaceous porous media at ventilation experiment, Mont Terri. Journal of Rock Mechanics and Geotechnical Engineering; 5 (2). http://dx.doi.org/10.1016/j.jrmge.2013.02.002
13. Bond A, Benbow S, Wilson J, Millard A, Nakama S, English M. (2013c) Reactive and nonreactive transport modelling in partially water saturated argillaceous

porous media around the ventilation experiment, Mont-Terri. Journal of Rock Mechanics and Geotechnical Engineering;5(1). http://dx.doi.org/10.1016/j.jrmge.2012.06.001

14. Bond A and S Watson (2012). Understanding the Post-Closure Thermal Impact of HA/SF Waste Packages. Quintessa Report for NDA RWMD QRS-1384Q-R2 v2.1. http://www.nda.gov.uk/publication/qrs-1384q-r2-v2-1/
15. Quintessa (2013). QPAC: Quintessa's general-purpose modelling software. Quintessa Report QRS-QPAC-11 June 2013 (www.quintessa.org/qpac-overview-report.pdf).
16. Byrne GD and AC Hindmarsh, (1975). “A Polyalgorithm for the Numerical Solution of Differential-Algebraic Equations”, ACM Trans. Math. Software 1, pp 71-96